

Journal of Alloys and Compounds 452 (2008) 273-278



www.elsevier.com/locate/jallcom

Corrosion and oxidation behavior of Pr-based bulk metallic glasses

Q.G. Meng, S.G. Zhang, J.G. Li*

School of Materials Science and Engineering, Shanghai Jiao Tong University, Shanghai 200030, China Received 13 October 2006; received in revised form 29 October 2006; accepted 1 November 2006 Available online 30 November 2006

Abstract

The corrosion behavior of the quaternary Pr–Cu–Ni–Al bulk metallic glasses (BMGs) in 3.5 wt.% NaCl solution were investigated by potentio-dynamic polarization and electrochemical impedance spectroscopic techniques. It is found that the there is a good correlation between the corrosion resistance and the glass-forming ability (GFA) in the BMGs, the larger the GFA, the stronger the corrosion resistance. In case of the representative Pr₅₅Cu₁₅Ni₁₅Al₁₆ BMG, the isothermal heat treatment was conducted and it was found that the corrosion resistance became smaller with holding time at 483 K. The thermogravimetry measurement on the Pr–Cu–Ni–Al BMGs showed that the oxidation resistance was deteriorated by increasing the Cu content and no correlations were found with the GFA. The composition of the scales formed during the oxidation was confirmed by X-ray diffraction. The corrosion and oxidation mechanisms were also discussed based on the experimental results.

Keywords: Amorphous materials; Corrosion; Glass-forming ability; Oxidation

1. Introduction

Since the first "bulk metallic glass" (BMG) Pd–Cu–Si was prepared by Chen in 1974 [1], many families of the bulk metallic glass-forming alloys including La–Al–Ni, Zr–Ti–Cu–Ni–Be, Zr–Ni–Al–Cu, Mg–Cu–Y and Pd–Cu–Ni–P have been discovered in the early1990s [2–5]. These new BMGs are expected to open up extensive applications due to their unique structures and properties. Among these, the rare-earth (RE) based BMGs offer great potential for application as functional materials [6,7].

For practical application of the RE-based BMGs, an understanding of the corrosion and oxidation behavior is needed. However, little work has been done on this topic. It is reported that many amorphous alloys has superior corrosion resistance due to their special structures without crystal boundary. Alvarez et al. [8] had explored the corrosion behavior of Ni–B–Sn melt-spun amorphous ribbons in NaCl solution with different pH values using Tafel experiments, and concluded that this amorphous alloy exhibits a better corrosion resistance than the crystalline counterpart; Qin et al. [9] used X-ray diffraction (XRD), Electrochemical impedance spectroscopy (EIS) and X-ray photoelectron spectroscopy (XPS) to monitor the

corrosion behavior of $Zr_{55}Al_{10}Cu_{30}Ni_{5-x}Pd_x$ (x=0, 5 at.%) BMG. The results showed that the difference in the corrosion behavior is originated from different glass-forming ability (GFA). On the other hand, only several investigations of oxidation behavior of conventional amorphous alloys (e.g. Zr-based and Fe-based amorphous alloys) are reported in the literature [10–13]. They considered that the oxidation behavior of the glass-forming alloys strongly depended on the alloy composition and microstructures. The oxides are likely to be formed first for the composition elements with large quantity and strong affinity for oxygen.

In this study, we focus on the corrosion and oxidation behavior of Pr–Cu–Ni–Al BMGs, and particularly on understanding the role of amorphous structure and alloy composition in the corrosion and oxidation mechanisms. Moreover, it is of interest to make a comparison between the corrosion and oxidation mechanisms as they are in nature all oxidation–reduction processes.

2. Experimental

The Pr-based master alloys with the nominal atomic percent compositions were prepared by arc melting Cu, Ni, Al with the purity of no less than 99.9 wt.% and Pr with the purity of no less than 99.7 wt.% in titanium-gettered argon atmosphere. Cylindrical specimens of 2 mm in diameter and 60 mm in length were prepared from the pre-alloys ingots by suction casting into a copper mold. The heat treatments were carried out in an evacuated quartz tube with a vacuum of 1×10^{-3} Pa. Thermal analysis was performed from the room temperature

^{*} Corresponding author. Tel.: +86 21 62932569.

E-mail addresses: mggsjtu@sjtu.edu.cn, lijg@sjtu.edu.cn (J.G. Li).

to the liquidus temperature (T_1) at a constant hearting rate of 10 K/min with a differential scanning calorimeter (DSC, Netzsch DSC 404C). The microstructure of samples was examined by XRD in a D/Max-rB diffractometer using Cu K α radiation.

The cylindrical specimens for electrochemical tests were ground into an area of $0.2 \,\mathrm{cm} \times 0.5 \,\mathrm{cm}$ at one end and a copper wire lead was attached with the silver paint to the other end. Except for the exposed surface for testing, the entire specimen was covered with an epoxy resin. The testing areas were mechanically polished with successive SiC papers of 240, 400 and 600 grain size, then were degreased with ethyl acetate and were washed with ethyl alcohol and distilled water before each experiment. Electrochemical measurements were carried out using a typical three-electrode system: a stationary specimen, a pair of counter electrodes (made of Pt sheet) and a saturated calomel reference electrode (SCE). A CHI 660 A electrochemical workstation was used for the polarization curves and the electrochemical impedance spectroscopy (EIS) measurements at room temperature after 20 min exposure to the test solution starting at the open-circuit potential. The test solution, 3.5 wt.% NaCl aqueous solution, was prepared with analytical grade NaCl reagent (≥99.5 wt.%) and deionized water. A scan rate of 0.8 mV/s was used for the potentiodynamic polarization test. The EIS method was used in the frequency range from 10⁵ to 0.1 Hz and involved the imposition of a sine wave with 5 mV in amplitude. From potentiodynamic polarization curves and EIS results, the parameters related to corrosion were then obtained to analyze the electrochemical behavior of these BMGs. The BMGs for the oxidation experiments were sliced into Ø $4 \, \text{mm} \times 0.5 \, \text{mm}$ and the experiments were carried out in dry air using a thermogravimetry analyzer (TG, Netzsch TG209).

3. Results

3.1. DSC measurement

Fig. 1 shows typical examples of DSC results for the ascast Pr-Cu-Ni-Al BMGs in cylindrical shapes at a heating rate of 10 K/min. These alloys reveal sequential phase transition from amorphous state to the glass transition region, supercooled liquid region, fully crystallized state and melting region. The supercooled liquid region $\Delta T_{\rm x}$ (= $T_{\rm x}-T_{\rm g}$) [14] became smaller and the crystallization process was split into two peaks in the sequence from Pr₅₄Cu₁₅Ni₁₅Al₁₆ to Pr₆₀Cu₅Ni₂₅Al₁₀ BMGs in Fig. 1, where the T_g and T_x represent the onset temperatures of glass transition and crystallization, respectively. All of the related thermodynamic parameters deduced from the DSC curves of Fig. 1 are summarized in Table 1. Many criterions have been proposed to evaluate the GFA [14–16], If ΔT_x and $\gamma = T_x/(T_g + T_1)$ [16] are used as indicators of the GFA for the Pr–Cu–Ni–Al BMGs, it is obvious to see that ΔT_x and γ have the same tendency with compositions, and the GFA ranks from high to low as the following: $Pr_{54}Cu_{15}Ni_{15}Al_{16} > Pr_{60}Cu_{25}Ni_{5}Al_{10} >$ $Pr_{60}Cu_{20}Ni_{10}Al_{10} > Pr_{60}Cu_{10}Ni_{20}Al_{10} > Pr_{60}Cu_{5}Ni_{25}Al_{10}$.

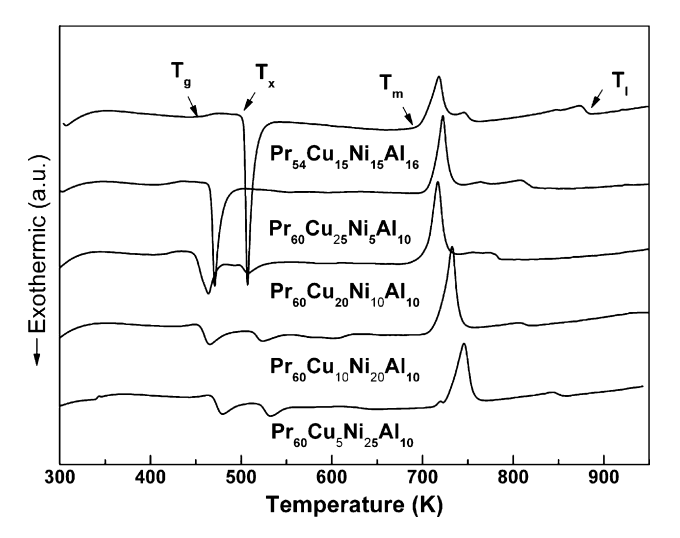


Fig. 1. DSC traces for Pr–Cu–Ni–Al bulk metallic glasses with the diameter of 2 mm at a heating rate of 10 K/min.

3.2. Electrochemical impedance spectroscopy

The impedance data of Pr-Cu-Ni-Al alloys in 3.5% NaCl solutions at room temperature were obtained after holding the samples at open-circuit potential for 20 min. Thus, it made all the samples get a stationary open-circuit potential before the test of EIS and potentiodynamic polarization experiments. Just like the Pr₆₀Cu₅Ni₂₅Al₁₀ Nyquist plot in Fig. 2(a), all the resulting Nyquist plots of Pr–Cu–Ni–Al alloys (Figs. 3 and 4) present only one capacitive loop, which are confirmed by the Bode plot of the impedance data in Fig. 2(b). The sole peak of the phase curve corresponds to the capacitive loop in the whole range of the experimental frequency. Then, we adopted several equivalent circuit models containing only one capacitive loop to fit the impedance data for such alloy system. The best fitting model can be represented by the equivalent circuit R(QR) (the inset of Fig. 2(a)) composed of one parallel RQ arrangement in series with the ohmic resistance whose mathematical expression of the impedance is given by:

$$Z = R_{s} + \frac{1}{j\omega Q_{dl} + (1/R_{t})} = R_{s} + \frac{R_{t}}{1 + j\omega R_{t}Q_{dl}}$$
(1)

where R_s is the solution resistance, $Q_{\rm dl}$ the non-ideal double layer capacity and $R_{\rm t}$ is the electrochemical transfer resistance [17]. The constant phase elements, $Q_{\rm dl}$, were used instead of pure capacities, $C_{\rm dl}$, to represent the capacitive elements, taking account of the deviations of the system from the ideal state due

Table 1 Thermal properties deduced from the DSC measurements at a heating rate of 10 K/min, the values of the glass transition temperature T_g , the onset temperature of crystallization T_x , the onset melting temperature T_m , the offset melting temperature T_l , the supercooled liquid region ΔT_x and γ (= $T_x/(T_g + T_l)$) for the Pr–Cu–Ni–Al bulk metallic glasses

BMGs	$T_{ m g}$	T_{x}	$T_{ m m}$	T_{l}	$\Delta T_{ ext{x}}$	γ
Pr ₅₄ Cu ₁₅ Ni ₁₅ Al ₁₆	465.4	515.5	696.7	882.3	50.1	0.383
Pr ₆₀ Cu ₅ Ni ₂₅ Al ₁₀	417.6	465.8	707.1	819.7	48.2	0.376
$Pr_{60}Cu_{10}Ni_{20}Al_{10}$	413.9	449.0	689.9	784.8	35.1	0.374
$Pr_{60}Cu_{20}Ni_{10}Al_{10}$	435.0	454.4	707.4	819.3	19.4	0.362
Pr ₆₀ Cu ₂₅ Ni ₅ Al ₁₀	450.5	467.1	714.3	854.5	16.6	0.358

Download English Version:

https://daneshyari.com/en/article/1624697

Download Persian Version:

https://daneshyari.com/article/1624697

<u>Daneshyari.com</u>